

Evaluation of the Effect of Pitched Blade Impellers on the Performance of an Electrochemical Reactor

Rodríguez-Arias Yonatan¹, Alonzo-García Alejandro², Mendoza-Escamilla Victor³, Gutiérrez-Torres Claudia del Carmen⁴, Jiménez-Bernal José Alfredo⁵, Mollinedo Helvio⁵ and Martínez-Delgadillo Sergio^{6*}

¹ SEPI. ESIME Zacatenco, Instituto Politécnico Nacional. G.A. Madero, CP 07738, México D.F. México. Tel. (525)57296000, ext. 54586.

² Tecnológico Nacional de México - Instituto Tecnológico de Mérida, Departamento de Metal-Mecánica. Av. Tecnológico km. 4.5 s/n CP 97118. Yucatán. Mexico. Tel.(052)9999645000 ext. 11401

³ Depto. Electrónica, Universidad Autónoma Metropolitana Azcapotzalco. Av. San Pablo 180. Azcapotzalco. CP 07740, México D.F. México. Tel. (525)5319550 ext. 1081.

⁴Instituto Politécnico Nacional, LABINTHAP-SEPI. ESIME, U.P. Adolfo López Mateos, México D.F., Mexico. G.A. Madero, CP 07738, México D.F. México. Tel. (525)57296000, ext. 54586.

⁵ UPIITA, Instituto Politécnico Nacional. Av. IPN 2580, G.A. Madero, CP 07340, México D.F. México. Tel. (525)57296000 ext. 56862.

⁶ Depto. Ciencias Básicas, Universidad Autónoma Metropolitana Azcapotzalco. Av. San Pablo 180. Azcapotzalco. CP 07740, México D.F. México. Tel. (525)53189007.

*E-mail: samd@correo.azc.uam.mx

Received: 2 June 2016 / Accepted: 26 September 2016 / Published: 10 November 2016

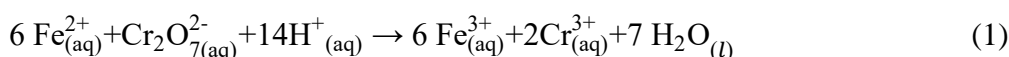
The use of electrochemical reactors to remove hexavalent chromium (Cr(VI)) in aqueous media, has shown remarkable results and it can be considered as a potential clean technology. In order to increase the reactor performance, its hydrodynamics must be studied. In this work, an electrochemical reactor with rotating rings electrodes and inner impellers added to the drive shaft has been proposed. Its performance was evaluated by CFD simulations, for different arrays of impellers at different rotational speeds. Although power consumption increased for higher speeds, vorticity and turbulence intensity were also increased inside the rotating rings electrode, thus improving the hydrodynamic performance of the reactor..

Keywords: Electrochemical reactors, Computational Fluid Dynamics, pitched blade impellers, hexavalent chromium

1. INTRODUCTION

It has been long recognized that Cr(VI) is one of the most hazardous pollutants present in industrial wastewaters [1-3.]. A wide variety of treatments have been applied to remove this hazardous

pollutant but most commonly used treatments require the addition of chemical reagents and generate considerable amounts of sludge, as a result their maintenance and operational costs are high [3-5]. Although there exist newer treatment processes, they also require reagents or adsorbents which have to be regenerated or replenished to maintain the process. Some of these solutions also require expensive materials, such as platinum, carbon nanotubes, etc. Moreover, the newly proposed treatments mostly evaluate the removal capacity of the process and therefore are not ready for plant scale usage [3-5]. The electrochemical process can be advantageously used to decrease Cr(VI) concentration to meet the required environmental levels, because it reduces Cr(VI) to Cr(III) without using chemical reagents, which reduces sludge production [6-8]. The reaction 1, shows the Cr(VI) reduction process [5]. It starts when Fe^{2+} is released from anode into the bulk liquid during the electrochemical process.



Another reaction is the one of Fe^{2+} regeneration on the cathode that contributes to the Cr(VI) reduction and makes the process more efficient [7]. Both species, Cr^{3+} and Fe^{3+} are precipitated and removed from the treated wastewater. After Cr(VI) removal, the treated wastewater can be reused in the industry (e.g. as rinsing water) and the sludge produced by this process, can be treated to separate the Cr^{3+} from the Fe^{3+} , and then both can be reused as well, making this process a potential clean technology. However, during the electrochemical process an iron oxide salt film is formed on the electrodes surface (electrode passivation) that can reduce the process efficiency and mass transfer that reduces Cr(VI) removal efficiency and causes greater energy consumption [6-8]. This effect is significant for reactors with stationary electrodes [8]. Passivation results in poor diffusion. Consequently, electrochemical reactors have to be designed to reduce passivation and to have higher mass transfer between the electrodes and the bulk liquid. Modeling this type of reactors using computational fluid dynamics (CFD) tools has proven to be very useful. Hydrodynamic behavior can be accurately predicted by CFD [9-12] and used to estimate the mixing time for various operating speeds thus providing design methodologies to enhance reactor performance [13]. In previous works an electrochemical reactor with rotating rings electrodes was evaluated. However, CFD results showed that the flow field was not homogeneous and it presented a zone inside the rotating electrodes which had low values of velocity, turbulence and vorticity thus reducing mass transfer and process efficiency [6, 14]. The use of impellers has been studied in several research works which show its beneficial influence on process performance [15-17]. In this paper an array of two pitched blade impellers were placed inside the electrodes ring assembly, as shown in Figure 1. In order to evaluate impellers influence, different parameters such as turbulence intensity, vorticity magnitude and axial velocity were evaluated by using state-of-the-art CFD tools [18-20] at different rotational speeds. Simulation results were experimentally validated measuring power consumption.

2. METHODS

The electrochemical reactor is formed by an arrangement of 14 iron ring electrodes. Electrodes are evenly distributed one cathode followed by one anode (7 cathodes and 7 anodes). The distance

between rings is 17 mm. The reactor height was 0.367m and internal diameter of 0.27 m with a volume capacity of 18 L. The cylindrical tank has a torispherical bottom with four baffles symmetrically distributed. The main shaft is driven by a variable speed motor that controls rotational speed of the whole arrangement. Two impellers were added inside the rotating rings to improve mixing.

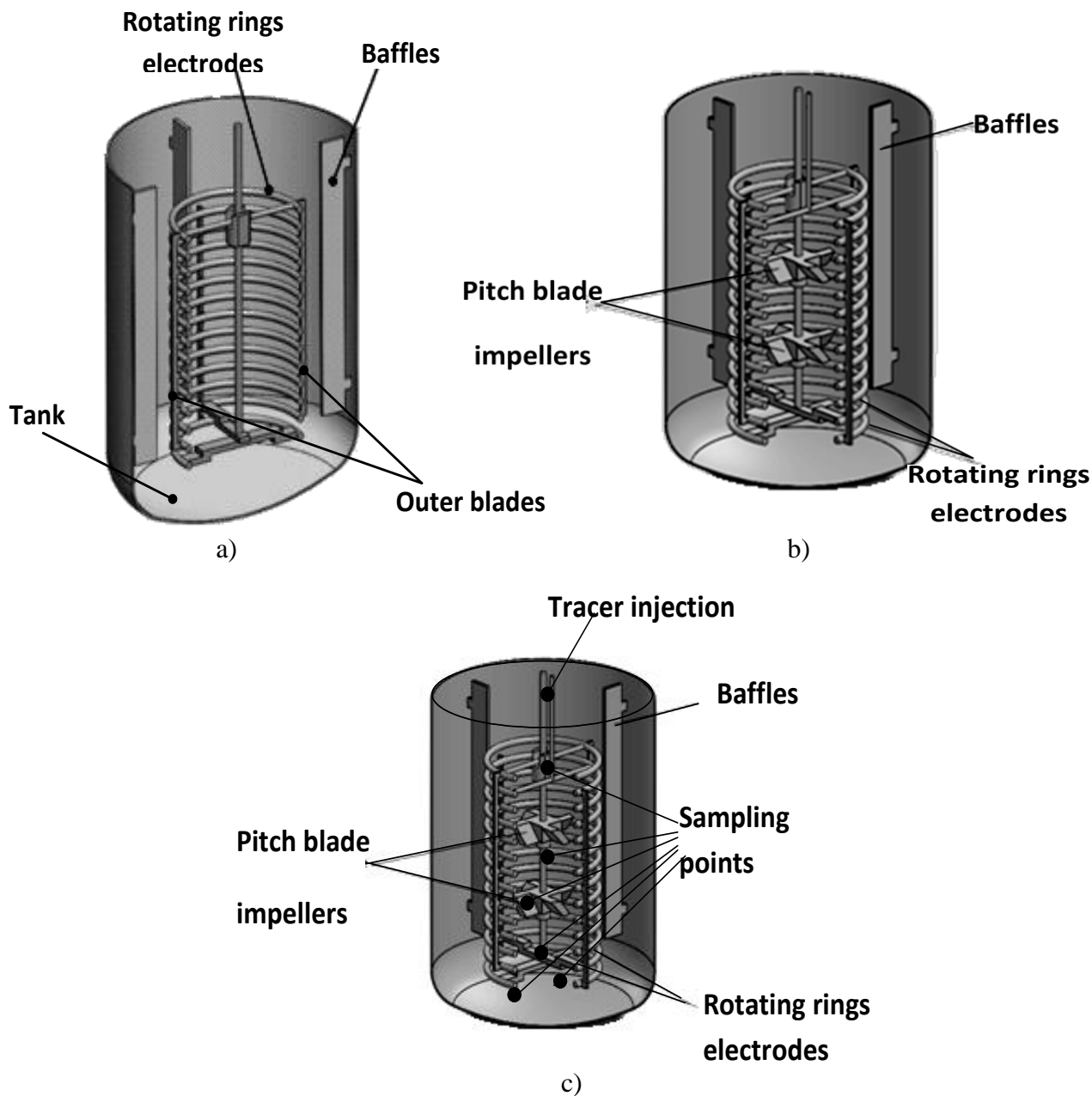


Figure 1. Electrochemical reactor with rotating rings electrodes: a) without impellers, b) with pitched blade impellers and c) injection and sampling points for mixing time (t_{99}) evaluation.

The effect of the rotational speed, of the electrode rings and impellers, on the performance of the reactor was evaluated. Tests were carried out with the rings electrodes rotating at 0 rpm, 150 rpm, 230 rpm and the impellers at 150 rpm and 500 rpm. The reactor height was 0.367m and internal diameter of 0.27 m with a volume capacity of 18 L. The reactor performance was evaluated with two impellers placed inside the rotating ring electrodes Two relative positions between both impellers

were tested. Case A, consist of both impellers fitted in a parallel arrangement and for case B one impeller was rotated 45° respect to the other (Case B). The results were compared against the reactor without impellers. The power consumption (P) was evaluated experimentally at different rotational speeds in the three cases. Differences between the experimental data and CFD simulation were less than 5%. CFD calculations were performed as follows [21, 22]:

$$P = \omega \int_A r \times (T dA) \quad (2)$$

where: A is the overall area of both, the rotating rings electrode and shaft surface, ω is the angular velocity vector, r the position vector and T the stress tensor. Tests and simulations were performed with the electrodes and impellers rotating at the different conditions and speeds as shown in Table 1.

Table 1. Reactor arrangements; rings electrodes and impellers rotating speeds tested

Reactor arrangement	Test 1	Test 2	Test 3	Test 4	Test 5	Test 6
Rotating rings electrodes	150 rpm (without impellers)	150 rpm	150 rpm	230 rpm (without impellers)	0 rpm	150 rpm
2 parallel aligned impellers (Case A)	--	150 rpm	--	--	500 rpm	500 rpm
2 impellers rotated 45° respect to each other (Case B)	--	--	150 rpm	--	--	--

Fluent[®] CFD software was used to simulate the different reactor configurations under test. In all the cases, a three dimensional model was used. Due to geometrical complexity, the models were meshed using tetrahedral elements. Grid independence analysis was performed and models were selected bearing in mind the balance between mesh density and computational time. Simulations were programmed using a pressure-based segregated algorithm. The standard scheme was used for pressure discretization, a second order upwind scheme was applied for momentum discretization and the semi implicit pressure-linked equation (SIMPLE) algorithm for pressure-velocity coupling. Multiple Reference Frame (MRF) approach was used to model steady-state flows inside the reactor [23]. The solution domain was divided into inner regions containing the rotational parts (impellers and/or the ring electrodes) and an outer region containing the stationary tank with baffles. Simulations were solved using the realizable κ - ϵ model. For the continuity equations a convergence criterion of 1×10^{-5} was reached; for the velocity components and for the κ - ϵ equations, the convergence criterion reached was 3×10^{-4} . Additional controls for convergence were set up to ensure stable values of dynamic pressure and torque in previously defined regions. Simulations with four meshes, with different cell density, were performed to check grid independence (Figure 2).. Torque, which was calculated, for each case, using the total moment, was chosen as the leading parameter for the mesh independence check due to the importance the global energetic efficiency of the device. The grid used for simulation

had 1547210 cells, cells, because a denser mesh only increased the simulation time and they did not change simulation results by more than 5%, as can be seen in Figure 2.

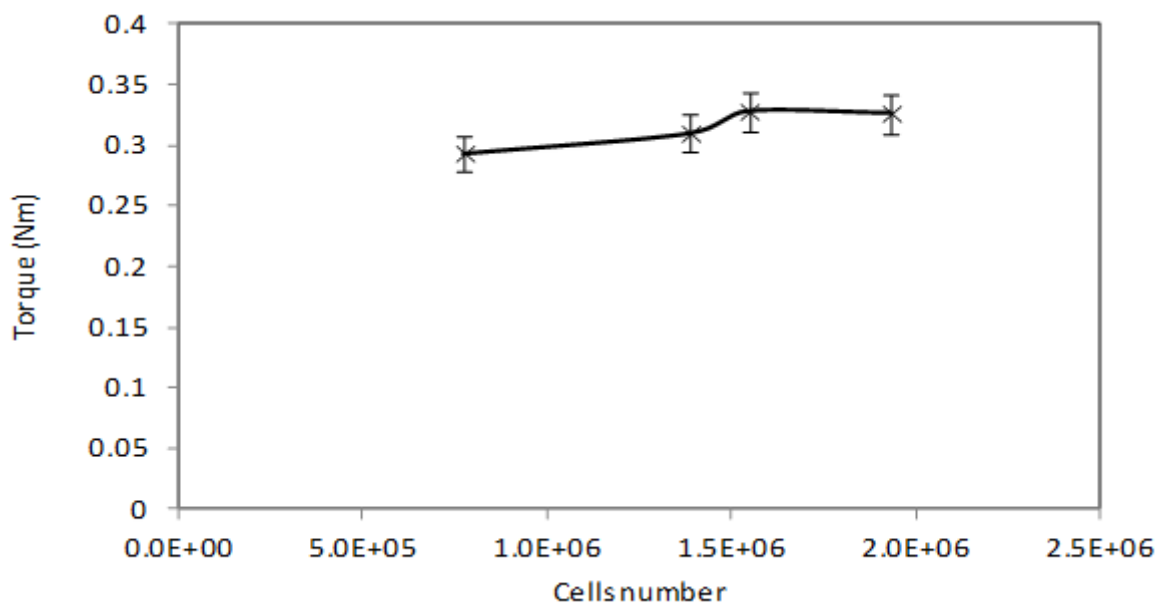


Figure 2. Mesh independence analysis (error bars of 5%).

Mixing time (t_{99}) was calculated, for all configurations and operational conditions, using a tracer pulse with the same physical properties as the bulk liquid. The tracer was added at the top of the reactor and its concentration was evaluated over time in different points inside the reactor (shown in Figure 1c). The uniformity U was evaluated based on the coefficient of variation (C_{OV}), which is the ratio between standard deviation σ_Y and the average (\bar{Y}), as shown in equations 5 and 6, respectively.

$$C_{OV} = \frac{\sigma_Y}{\bar{Y}} \tag{5}$$

$$U = 1 - C_{OV} \tag{6}$$

3. RESULTS AND DISCUSSION

Axial velocity contours obtained by CFD are shown for the three cases in Figure 3. For the original case with no impellers (Figure 3a), flow dynamics imposed by rings rotation create two primary structures: a radial flow from electrodes that increases dynamic pressure towards the wall of the tank, while creates another zone of low dynamic pressure in the central part of the reactor (downward axial flow). Interaction of these zones creates secondary structures such as the large eddies located at mid-height close to the wall of the tank (red dashed ovals).

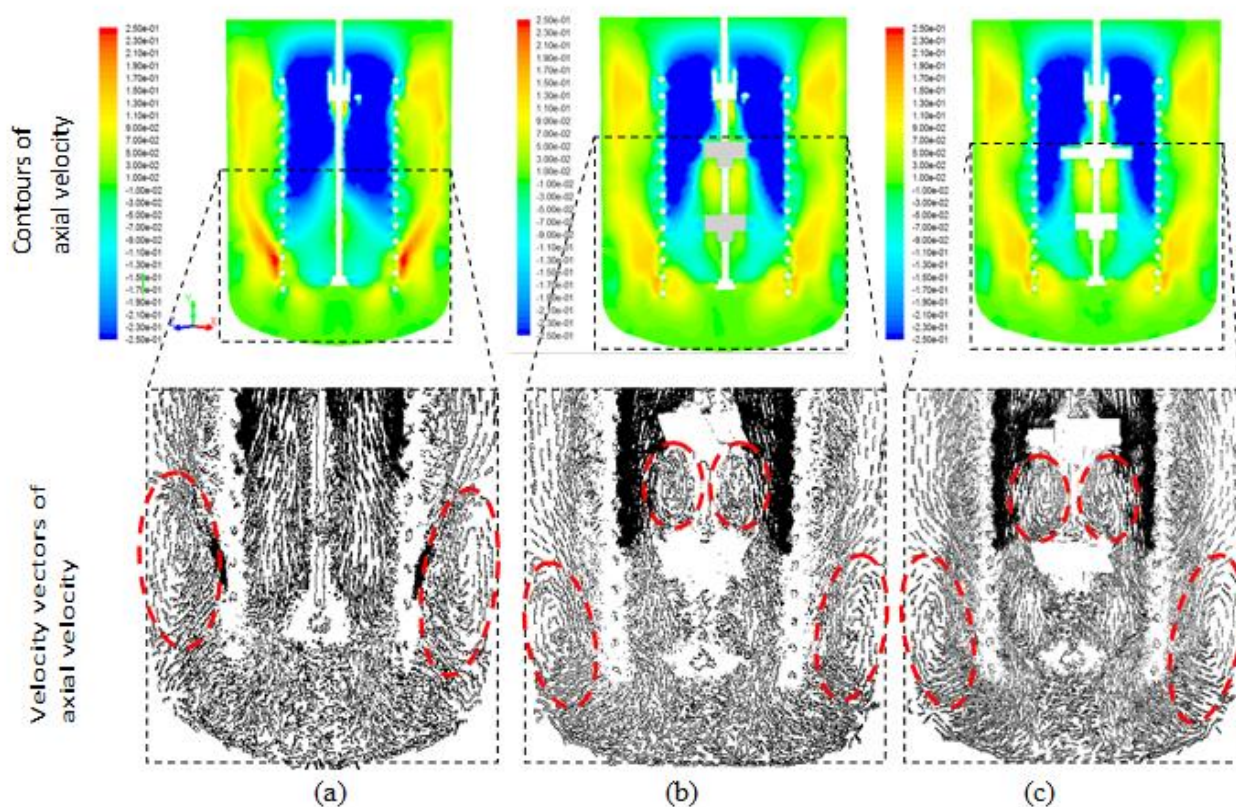
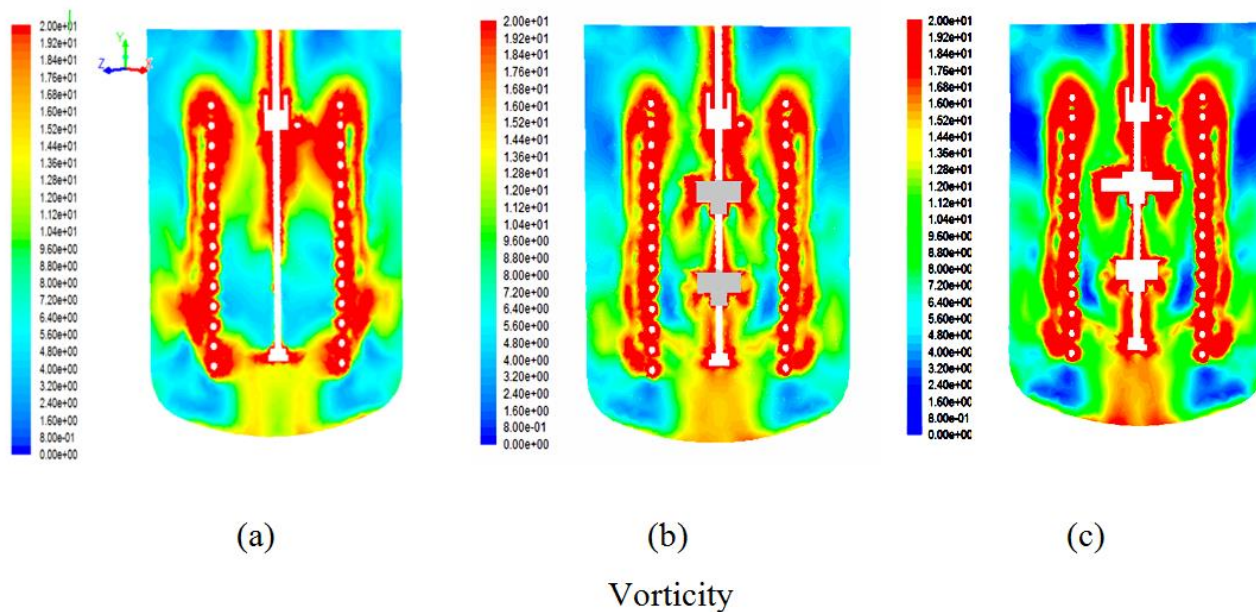


Figure 3. Contours maps and velocity vectors of axial velocity for the three cases: a) with no impellers, b) aligned impellers (case A) and c) 2 impellers rotated 45° respect to each other (case B) at 150 rpm.



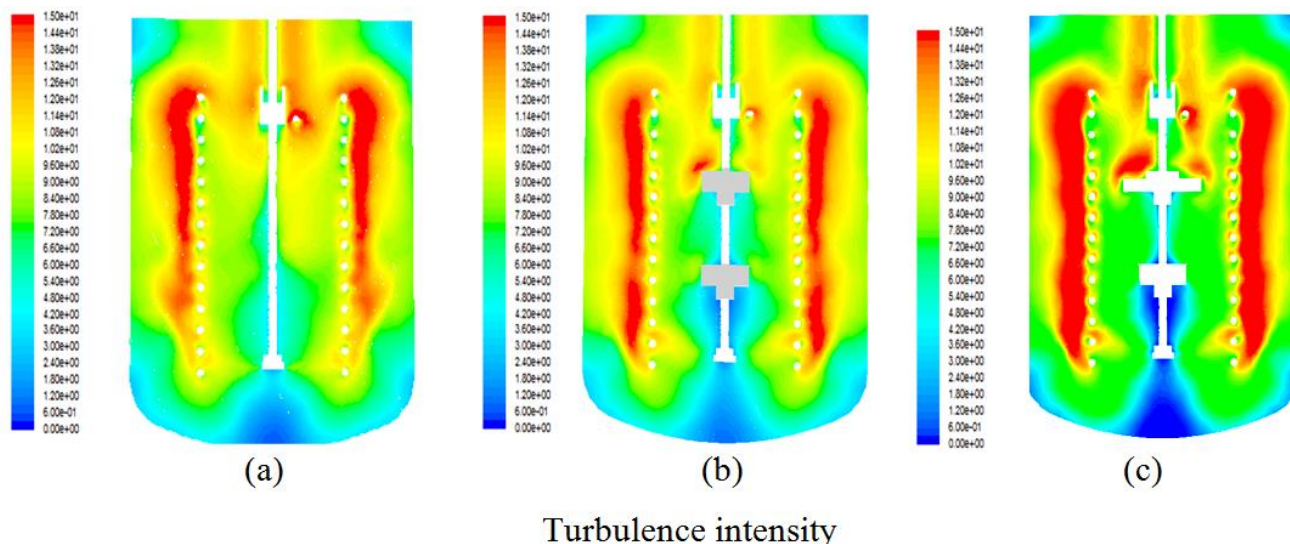


Figure 4. Vorticity field and Turbulence intensity for the three cases: a) with no impellers, b) 2 impellers (case A), and c) 2 impellers rotated 45° respect to each other (case B) at 150 rpm.

The lower pressure in the central part of the reactor is extended towards its base, causing a decrease in the momentum exchange due the diffusion and dissipation mechanisms induced by the fixed recirculation zones. Also, as the flow moves to the bottom part of the reactor, it is blocked but no defined recirculation region is formed. When the impellers, in cases A and B (see Figure 3b and 3c), rotate at the same speed as the electrodes, they reduce the downward axial flow as evidenced by the reduced contours in blue. Such behavior is because impellers pumping capacity at 150 rpm is lower than the one imposed by the downward axial flow produced by the rotating rings.

Hence, downward flow is restricted by impellers. Moreover, the liquid pumped down by the upper impeller impacts on the lower impeller producing positive axial velocities between impellers (red-yellow zones), and therefore generating two new recirculation zones (red dashed ovals inside electrodes in Figure 3b and 3c). As a result of the previously referred phenomena, the vorticity increases near the impellers in both cases, as is depicted in Figure 4.

Clearly, impellers increased turbulent intensity, thus causing a better mixing compared to the configuration without impellers. On the other hand, in all cases, there exist low turbulence zones between the lower part of the rings and the bottom of the reactor. With the intention of reducing the zones of low turbulence and vorticity inside the rings for the reactor with no impellers, the rotational speed was increased to 230 rpm. Figure 5 shows the velocity contours at 230 rpm for such case. As can be seen, increased axial velocity, vorticity and turbulence intensity, are obtained in comparison with the tests performed at 150 rpm ((i.e., with no impellers and both cases A and B). Nevertheless, the zones with low velocity and vorticity inside the rotating rings electrode were still present.

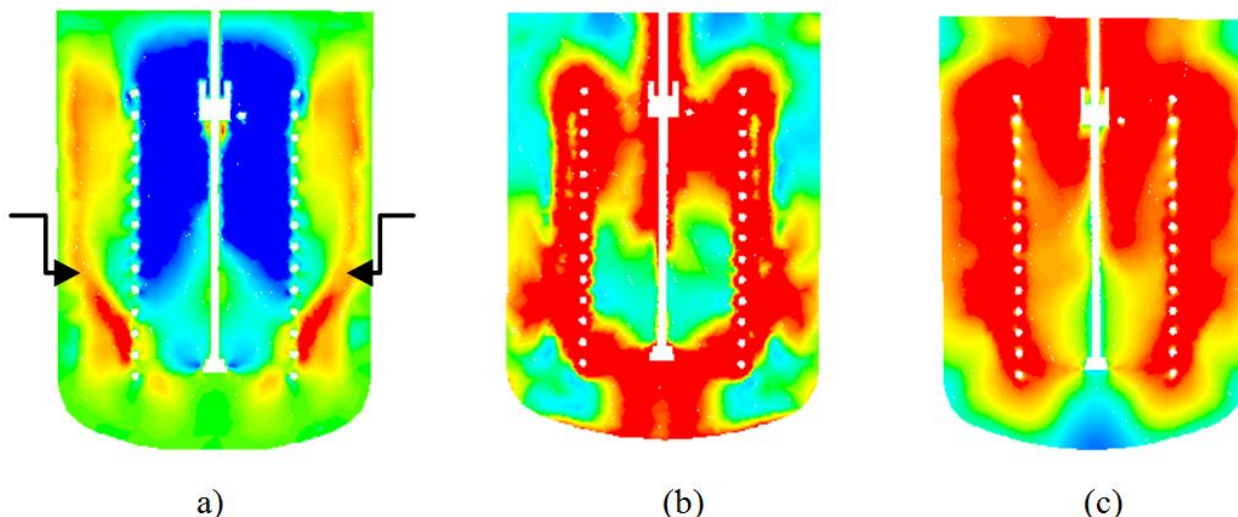


Figure 5. Velocity maps for the reactor with no impellers at 230 rpm: a) axial velocity (m/s) b) Vorticity magnitude (1/s) and c) Turbulence intensity (%).

Again, the blockage exerted against downward flow by the reactor bottom, creates a zone where flow is turbulent and energy is dissipated. This section contains a mass of liquid that is prevented from coming into contact with the electrodes, causing large dead zones and thus reducing the efficiency of the reactor. In addition, due to the higher rpm applied, the counter-rotating vortices, similar to those in figure 3a, formed between the walls of the reactor and near the last five bottom rings, increased in intensity constraining and accelerating the flow upward near the reactor walls that causes the maximum upward axial velocity that are present in the periphery, (shown in red and marked with the arrows in Figure 5a). Consequently, the maximum upward axial velocity is located in the aforementioned zone. In order to increase the turbulence intensity, vorticity, axial velocity and reduce the secondary flow in the lower section of the reactor, electrodes were kept stationary but impellers were added and its speed was increased from the previous 150 rpm to 500 rpm. (Figure 6), but in this case the rotating rings electrode was kept static (0 rpm). Once more, downward flow produced by the upper impeller is disrupted by the lower impeller because flow created by the upper impeller is higher than the flow that the lower impeller can pump at that condition (500 rpm).

Therefore, the lower impeller creates zones of positive axial velocity inducing the formation of two distinctive recirculation regions under it (orange-yellow zones, in Figure 6a and small red circles, in Figure 6b). These results of velocity vectors are similar to those obtained with two impellers at 100 rpm, but without rotating rings [24]. As can be seen in Figures 6c and 6d, the turbulence intensity is reduced under the lower impeller and the vorticity increased. Although the axial velocity, vorticity and turbulence increased inside the rings, it occurred only in the zone limited by the upper impeller and the lower end of the rings array.

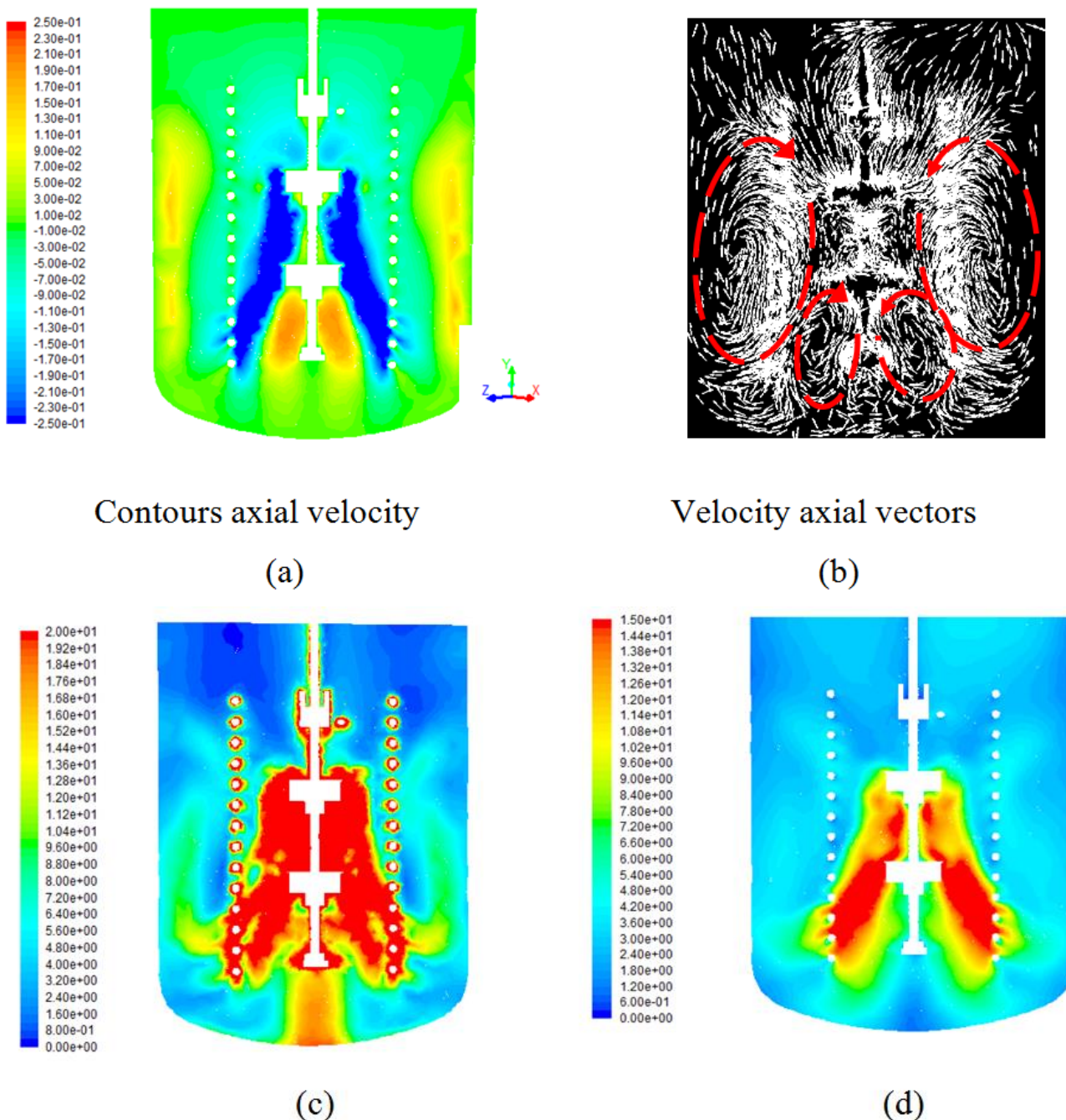


Figure 6. Velocity maps for the reactor with 2 impellers (case A) at 500 rpm and rings electrode was kept static (0 rpm): a) axial velocity contours and b) velocity vectors, c) vorticity magnitude(1/s) and d) turbulence intensity (%).

In addition, the main flow is restricted to the middle zone of the reactor (large red paths shown in the axial velocity of Figure 6b), causing the upper and bottom parts of the reactor to have a poor mixing condition. As can be seen, the velocity near the electrodes is low; hence the mass transfer between the electrodes and the bulk liquid will be small. Based on these results, a test was carried out rotating the impeller at 500 rpm while the rings were rotated at 150 rpm. Figure 7 show the results of axial velocity, vorticity and turbulence.

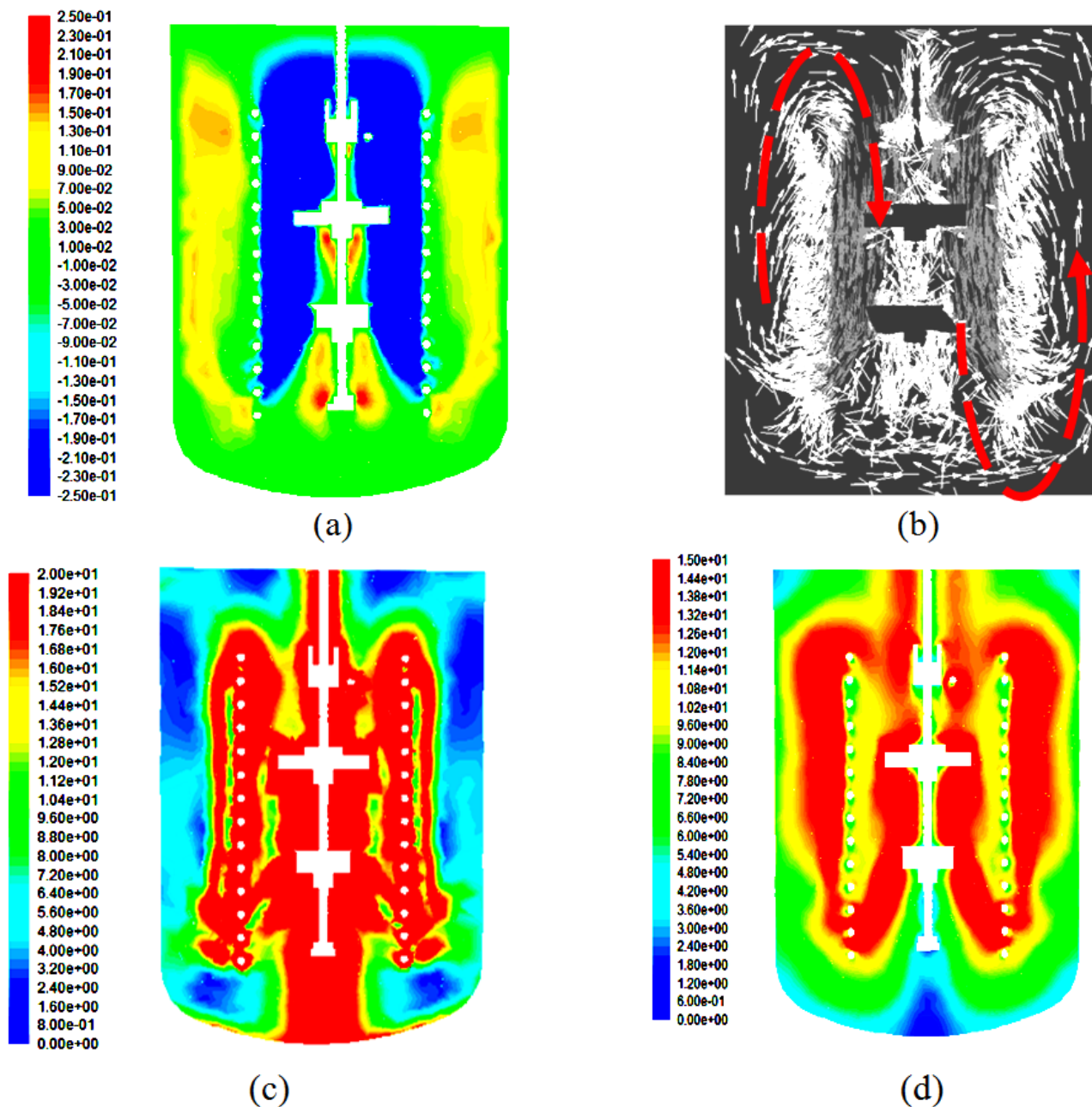


Figure 7. Performance of the reactor with 2 impellers at 500 rpm and rotating ring at 150 rpm: a) contours of axial velocity (m/s), b) velocity vectors, c) vorticity magnitude (1/s) and, d) turbulence intensity (%).

As it is shown, there is an improvement in those parameters. The downward flow rate inside the rotating ring electrode reaches deeper (Figure 7a and 7b) than in the other cases, in agreement with other authors [25], due to these kind of impellers have a strong axial circulation capacity. Moreover, the upward flow surrounding the electrodes create the highest mixing zone of all cases tested,. The vorticity and the turbulence intensity were noticeably increased (Figure 7c and 7d, respectively) inside the rotating rings, reaching higher values than in the other cases. However, small recirculation zones under the impellers appear (Figure 7a) and, due to the rotating flow in the bottom of the reactor the

vorticity is high (Figure 7c). The flow fields in the cases A and B presented no important differences for the same rpm tested in this work, then only the results of case A are presented.

In Figure 8, the turbulent dissipation rates for the different cases are compared. As can be seen, the turbulent dissipation rates occur in regions away from the outer blade of the rotating ring electrodes, but only in the case d) there is no energy dissipation in this zone due to the stationary condition of the ring electrodes. It is worth noting that for cases a) and b), turbulent dissipation rates are too low in the inner zone of the ring electrodes, whereas cases c) and d), show higher dissipation rates in the same zone. The difference is due to impellers high rotational speed, which enables efficient mixing, which is agree with other studies[26]. Moreover, case c) shows higher dissipation rate in the external zone of the rings, which implies better mixing and higher mass transfer rate.

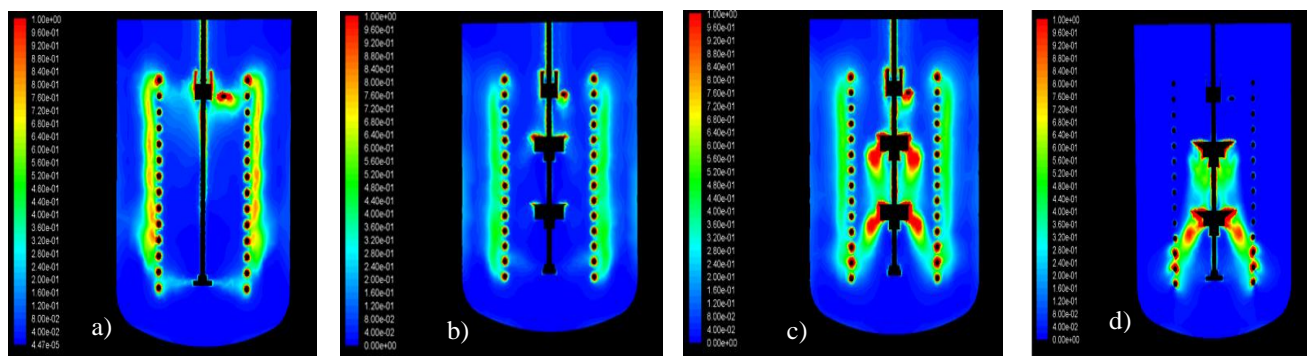


Figure 8. Turbulent dissipation rate (ϵ): a) Rotating rings at 150 rpm and no impellers, b) Rotating rings and impellers at 150 rpm, c) Rotating rings at 150 and impellers at rpm 500 rpm and d) Rotating rings at 0 rpm and impellers at rpm 500 rpm.

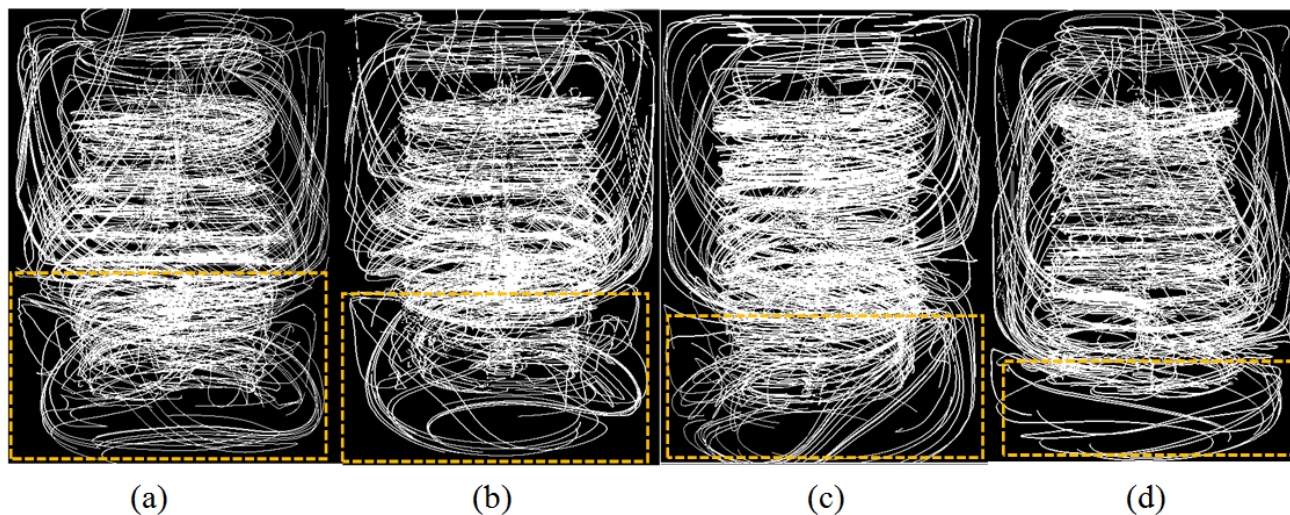


Figure 9. Axial velocity pathlines: a) with no impellers 150 rpm, b) with no impellers 230 rpm, c) 2 impellers at 150 rpm and rotating rings at 150 rpm and d) 2 impellers at 500 rpm and rotating rings at 150 rpm.

As the rotational velocity of the rotating rings electrodes and impellers increased, the lower recirculation zone (dashed line rectangles) in the reactor was reduced, as shown Figure 9. For the case of the reactor without impellers, increasing the speed from 150 rpm to 230 rpm of the rings electrode caused a small reduction in that zone (Figure 9a and 9b, respectively). On the other hand, when both impellers and electrodes rotated at 150 rpm the lower recirculation zone was further reduced (Figure 9c). The increase in the rotating velocity of the impellers from 150 rpm to 500 rpm, with the rings rotating at 150 rpm (Figure 9d), presented the highest effect in the reduction of the zone having an important effect on mixing that reduced the mixing time.

For every rotating condition tested in both cases A and B, the fluid momentum was increased. By changing the rotational speed, it was possible to influence the size, intensity and location of the recirculation regions. However, the use of impeller pairs present secondary effects such as the small vortices between them that consume system energy and reduce reactor pumping capacity. This is because both impellers rotate at the same speed and the upper impeller develops an absolute outlet speed that is greater than the inlet speed that the lower impeller can manage; creating a blockage that generates vortices and for all practical purposes the loss of the second pumping stage (lower impeller). Axial velocities for all cases tested in this work are presented in Figure 10.

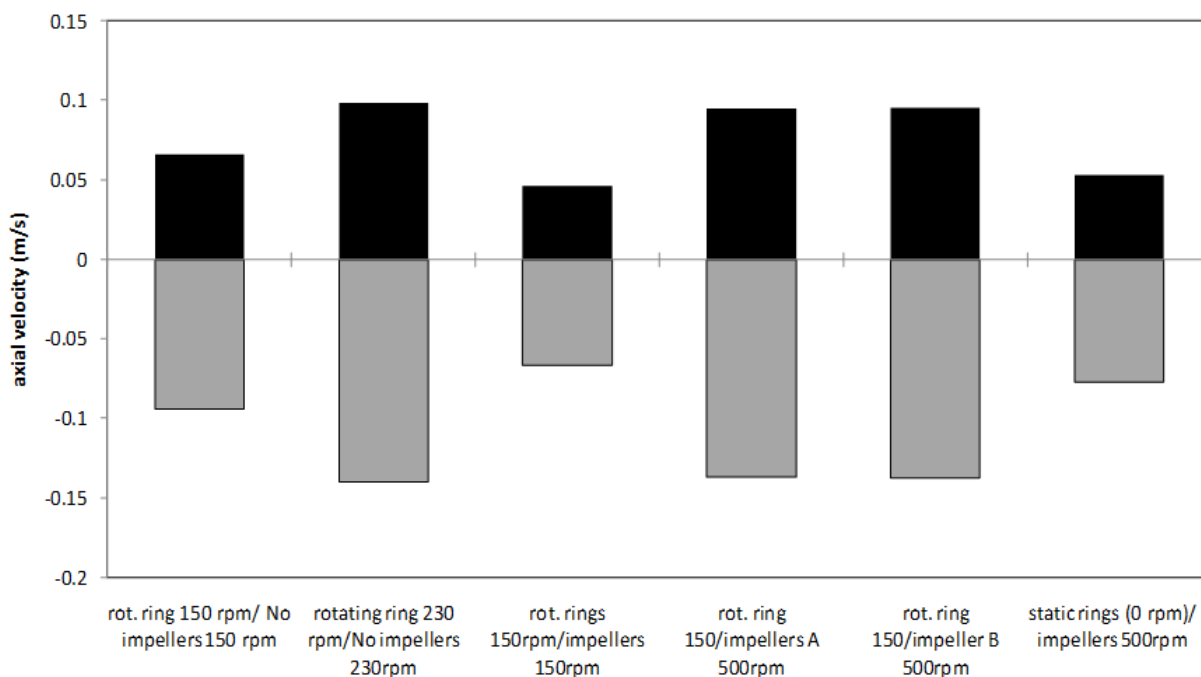


Figure 10. Axial velocity (m/s) for all cases tested.

As it is shown, higher axial velocity are reached when the reactor operates with the rotating rings and no impellers at 230 rpm and when the rotating ring rotates at 150 rpm and the impellers at 500 rpm, in both cases A and B. However, in the case of no impellers at 230 rpm, the downward mass flow rate does not reach the deeper section of the rings electrode (Figure 5a) as it does occur for the case with impellers. . Best results are obtained, when the rings rotate at 150 rpm and at the same time the impellers rotate at 500 rpm, downward mass flow reaches deeper, near the last ring of the electrode

(Figure 7a and 8d), improving mixing. Mixing time (t_{99}) measurements for all arrangements confirmed the last result. A pulse of tracer was used to measure concentration as a function of time in several sampling points (Figure 1c). Results of tracer mass fraction variation for each case are not presented, only those obtained for the case of impellers rotating at 500 rpm and electrodes at 150 rpm are presented in Figure 11.. Uniformity was evaluated and the mixing time (t_{99}) was calculated for all the cases (figure12). As can be seen in Figure 11b, at 3 s, the tracer is pumped down into the electrode rings by the impellers, and then, at the end of the rings, it is thrown towards the reactor walls improving the mixing. Tracer mass fraction time evolution is shown in Figure 11a, where after 12 s, 99% uniformity is reached..

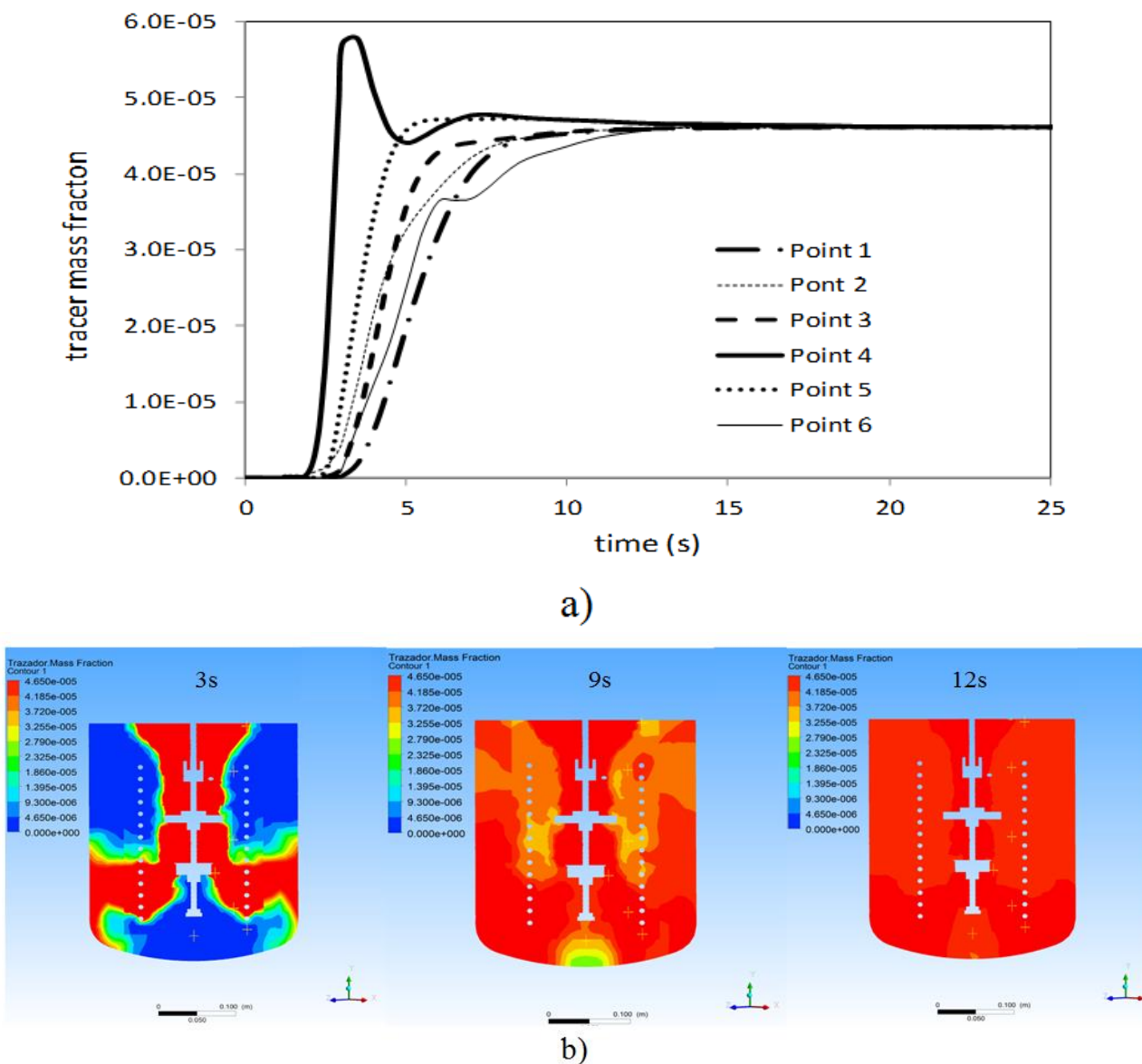


Figure 11. Reactor operated with the impellers rotating at 500rpm and the rotating rings at 150 rpm: a) Tracer mass fraction as a function of time and b) Tracer mass fraction contours at 3s, 9s and 12s.

Figure 12 shows the overall comparison of power consumption in the evaluated configurations, the reactor operating at 150 rpm with no impellers, causes the longest mixing time (25.5 s), and a low power consumption. For the same configuration at 230 rpm, the mixing time is reduced to 18 s, but has the disadvantage that it consumes the highest power. When the reactor is operated at 150 rpm (both, the impellers and the rotating rings) the mixing time was reduced to 15.5 s. Minimum mixing time, 12 s, is achieved when reactor is operated with impellers at 500 rpm and the rings at 150 rpm, although the power consumption increases in 30% in comparison with the reactor with no impellers at 150 rpm.

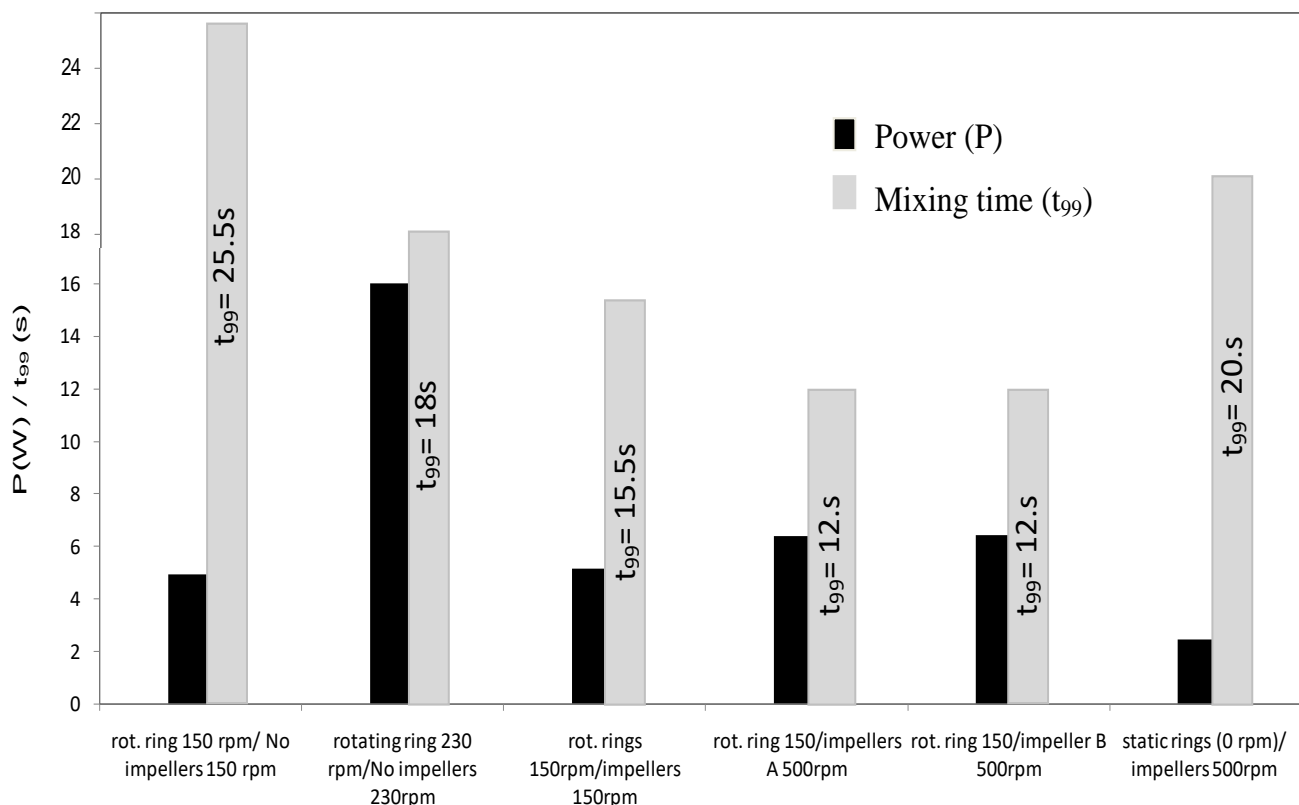


Figure 12. Power consumption (W) and mixing time (s), for the cases tested.

Finally, the reactor operated with the static rings electrode and impellers at 500 rpm, consumed the lowest power, but their mixing performance is deficient and the mixing time was 20 s.

4. CONCLUSIONS

CFD simulations allowed to obtain the dynamics that characterize all cases. For the original reactor configuration, it is found that rings rotation produce pumping towards the central zone of electrodes array and recirculation vortices on the outside. For this case, 150 rpm can be considered as the practical speed limit, because power consumption grows greatly for higher rotational speeds while mixing time reduction is not significantly diminished. So, it can be concluded that increasing rpm in

the original reactor is not a practical solution to improve mixing. Simulations clearly demonstrate that the addition of central impellers improve mixing inside the reactor by reducing the size and intensity of recirculation vortices. Such configurations increase pumping and enhance hydrodynamics, significantly decreasing mixing time (53%) by using a small power increment (16%). The best mixing and the lowest mixing time were accomplished when the impellers rotated at 500 rpm and the rings electrodes at 150 rpm, reaching the lowest mixing time (12 s). These improvements will allow for a higher volume water treatment. Results demonstrate the importance of hydrodynamic studies which have not received enough consideration in electrochemical science. Future designs will further explore the user of new impeller configurations.

ACKNOWLEDGEMENTS

Financial supports of this work by the Consejo Nacional de Ciencia y Tecnología (CB2011/169786) are gratefully acknowledged

References

1. L Liu and X. Ma . *J. Clean. Prod.*, 18 (2010) 1731.
2. M. Owlad, M Aroua, W. Daud, S. Baroutian, *Water Air Soil Poll.*, 1-4 (2009) 59.
3. C. Jung, J. Heo, J. Han, N. Her, S. Lee, J. Oh, J.Ryu and Y. Yoon, *Sep. Purif. Technol.*, 106 (2013) 63.
4. F. Fu, and W. Qi, *J. Environ. Manage.*, 92 (2011) 407.
5. M. Barakat, *M. Arab. J. Chem*, 4 (2011) 361.
6. S. Martinez-Delgadillo., H. Mollinedo, V. Mendoza-Escamilla and O. Huerta-Chavez, *Chem. Eng. Trans.*, 25 (2011) 315.
7. M. Rodríguez, R. Aguilar, G. Soto and S. Martínez, *J. Chem. Technol. Biotech.*, 78 (2003) 371.
8. S. Martinez and M. Rodriguez, *J. Chem. Technol. Biotech.*, 82 (2007) 582.
9. V. Ranade, *Chem. Eng. Sci.*, 52 (1997) 4473.
10. A. Sahu, P. Kumar, A. Patwardhan and J. Joshi, *Chem. Eng. Sci.*, 54 (1999) 2285.
11. D. Deglon and C. Meyer *Miner. Eng.*, 19 (2006) 1059.
12. R. Achouri, I. Mokni, H. Mhiri and P. Bournot, *Energ. Convers. Manage.*, 64 (2012) 633.
13. R. Leishear, S. Lee, M. Fowley, M. Poirier and T. Steeper, *J. Fluid Eng.*, 134 (2012) 1.
14. S. Martínez-Delgadillo, J. Ramírez-Muñoz, H. Mollinedo, V. Mendoza-Escamilla, C. Gutiérrez-Torres, and J. Jiménez-Bernal. *Int. J. Electrochem. Sci.*, 8 (2013) 274.
15. T. Kumaresan and B. Joshi, *Chem. Eng. J.*, 115 (2006) 173.
16. H. Furukawa, Y. Kato, Y. Inoue, T. Kato, Y. Tada and S. Hashimoto, *Int. J. Chem. Eng.*, 106496 (2012).
17. S. Roy and S. Acharya, *J. Fluid. Eng.*, 134 (2012) 1.
18. R. Thilakavathi, D. Rajasekhar, N. Balasubramanian, C. Srinivasakannan and A. Shoaibi, *Int. J. Electrochem. Sci.*, 7 (2012) 1386.
19. M. Vakili and M. Nasr-Esfahany, *Chem. Eng. Sci.*, 64 (2009) 351.
20. J. Derksen, *Flow Turbul. Combust.*, 69 (2002) 3.
21. A. Harvey, C. Lee and S. Rogers, *AIChE J.*, 41 (1995) 2177.
22. M. Li, G. White, D. Wilkinson and K. Roberts, *Chem. Eng. J.*, 108 (2005) 81.
23. W. Bujalski, Z. Jaworski and A. Nienow, *Chem. Eng. Res. Des.*, 80 (2002) 97.
24. J. Alfaro-Ayala, V. Ayala-Ramírez, A. Gallegos-Muñoz and A. Uribe-Ramírez, *Chem. Eng. Res. Des.*, 100 (2015) 203.
25. M. Chen, J. Wang, S. Zhao, C. Xu, and L. Feng, *Ind. Eng. Chem. Res.*, 55 (2016) 9054.

26. D. El-Gayar, A. Konsowa, Y. El-Taweel, H. Farag and G. Sedahmed, *Chem. Eng. Res. Des.*, 109 (2016) 607.

© 2016 The Authors. Published by ESG (www.electrochemsci.org). This article is an open access article distributed under the terms and conditions of the Creative Commons Attribution license (<http://creativecommons.org/licenses/by/4.0/>).